COBEM 2021 26th International Congress of Mechanical Engineering
ABCM Associação Brasileira de Engenharia e Ciências Mecânicas
November 22-26, 2021, Virtual Congress, Brazil

COB-2021-0259
NUMERICAL SIMULATION OF A HYBRID SYSTEM WITH PHOTOVOLTAIC PANELS, ELECTROLYZER AND SOLID OXID FUEL CELL

João Jun Okada Ahmed
Department of Agricultural and Environmental Engineering, Universidade Federal Fluminense (UFF), Rua Passo da Pátria, 156, Campus da Praia Vermelha, Bloco D, São Domingos, Niterói, RJ, CEP: 24210-240, BRAZIL
joao_jun@id.uff.br

Florian Pradelle
Department of Mechanical Engineering, Pontifícia Universidade Católica do Rio de Janeiro (PUC-Rio), Rua Marquês de São Vicente, 225, Gávea, Rio de Janeiro, RJ, CEP: 22453-900, BRAZIL
pradelle@puc-rio.br

Abstract. *With the increasing share of electricity from renewable sources in the energy matrix, it is important to improve the electricity supply and storage scheme, particularly for residential consumers, with a focus on efficiency, economic viability and sustainability. Thus, the present study investigates an isolated residential consumer using solar energy with hydrogen storage. The system gathers photovoltaic (PV) panels, an electrolyzer and a solid oxide fuel cell (SOFC) in order to supply the electrical demand of a residence. The energy surplus from the PV modules during periods of low demand is used for hydrogen production by water electrolysis and storage. The hydrogen is stored in tanks and used to fuel an SOFC to generate energy when the PV panels does not provide all electricity demand. Therefore, a simulator based on phenomenological model of the PV panels and fuel cell thermodynamics is developed in MATLAB software to analyze the energy and exergy efficiencies of the system on typical days. Based on the hourly solar irradiation and hourly demand profiles during a typical day of each season, the model allow to calculate the power and current in the PV modules, the amount of produced hydrogen (converting the surplus electric energy), the fuel flow rate required in the SOFC and, finally, the energy and exergy efficiencies of each stage, over a 24 hour period. This work proposes to evaluate the technical feasibility of this system under typical conditions of the city of Rio de Janeiro – RJ, Brazil. The results obtained by the numerical simulation present a production of 1.062, 0.320 and 0.0 kg/day hydrogen with the surplus electricity of the PV system, during summer, spring and winter, respectively. Also, the maximum total energy and exergy efficiencies are reported as 35.75% and 38.38%.*

Keywords: *Hybrid solar system, Hydrogen, Efficiency, Energy, Exergy*

1. INTRODUCTION

Sauthier *et al.* (2019) observed that Brazil, despite having its electric matrix mostly composed by renewable sources, mainly because of the large contribution of hydropower, has presented a rapid increase of solar energy investments and application over the past years, in particular since 2016. The photovoltaic (PV) panels are the main method to capture and convert solar irradiation into useful energy, consists of arrays of solar cells in series and parallel, responsible for producing current and voltage in the device. Each cell is composed of a p-n junction of semiconductor coated over a thin layer (or wafer), whose material is commonly Silicon (Si), due to its low cost and high availability (Sauthier *et al.*, 2019). Thus, as solar PV market grows and becomes mature, the PV modules efficiency increases, and its manufacturing costs decrease, due to technology improvement and lower costs material. Additionally, the PV materials recovery and recycling has been explored, reducing even more the environmental impacts in the whole life cycle (Tao *et al.*, 2015).

On the other hand, the hydrogen is considered one of the most promising fuels of the future, both for transportation and stationary applications. It presents a highest energy content per mass unit, which is 2.5 and around 3 times more energetic than methane and gasoline, respectively. The main methods to produce hydrogen can be classified by the raw material used, such as coal, natural gas, biomass or water. The last one is a renewable resource with a relative abundance that allow hydrogen production by electrolysis. It consists in applying a direct electric current to water to dissociate the molecules, obtaining hydrogen and oxygen. Polymer Electrolyte Membrane (PEM) electrolyzers, compared to solid oxide or alkaline electrolyzers, seems more suitable for low-scale applications. Despite the high investments costs, due to the membranes and the metal noble-based electrodes, this device produces very high purity hydrogen without the need of auxiliary equipment and has the ability to work under variable power feeding regimes. Nevertheless, with the material

costs decrease and technology advancement, the PEM hydrogen production capacity will further increase in the future (URSÚA et al., 2012).

Therefore, the fuel cell is an electrochemical device that converts the chemical energy of a fuel directly into electric energy through an oxidation-reduction reaction. These systems provide an efficient and clean mechanism for energy conversion, which can also be integrated to renewable sources and modern energy carriers – such as hydrogen – for sustainable development. The FC operates without noises or vibration, while its modularity allows for simple construction and a diverse range of applications in portable, transportation or stationary power generation. A proton exchange membrane fuel cell (PEMFC) can reach up to 40% of electrical efficiency while a solid oxide fuel cell (SOFC) has a maximum efficiency of 60% of electrical efficiency (Sharaf *et al.*, 2014).

In the past years, the hybridization of renewable energies, such as PV system, with hydrogen as a storage medium or complementary fuel has been gaining attention, since these systems are the only ones that produce large amounts of sustainable hydrogen with neither emission of pollutant gases nor consumption of fossil or nuclear resources (Dutta, 2014). Thus, solar photovoltaic (PV) energy technologies are constantly being improved to meet the current electrical demands, but it is still an intermittent energy source. In stationary applications, the use of energy storage, such as the production of hydrogen, a clean and attractive energy carrier, via water electrolysis from the surplus electricity, which can be converted into electric power when the demand surpasses the PV power, through a fuel cell (FC) can increase the system efficiency. Moreover, it is also possible to use the heat from the gas exiting the fuel cell in a combined heat and power (CHP) or combined cold heat and power CCHP unit. For instance, Hosseini *et al.* (2013) studied an integrated CCHP system with PV panels, electrolyzer, SOFC and an absorption chiller in order to provide all energy requirements from a 140 m² floor area Canadian residence. The simulated PV systems delivers a maximum power of 3.35 kW and allow the generation of 0.792 kg of hydrogen with the surplus electricity of the PV. The total energy and exergy efficiencies of the CCHP unit reach a maximum value equal to 55.7% and 49%, respectively. Gabriel (2020) introduced a numerical simulation of an on-grid hybrid system of a CHP unit for residential and industrial micro-applications. The system consists of a 5 kW PEMFC coupled to a natural gas reformer, PV panels and Pb-acid batteries connected to the grid. Paybacks between 6 and 20 years of system's operation were achieved. Finally, reductions in CO_2 emissions of up to 30% compared to those of the electricity from the Brazilian energy matrix and heat supply from burning natural gas were obtained when cogeneration from CHP unit was accounted to meet the consumers' thermal demand.

Evaluating integrated arrangements of solar PV-hydrogen systems and fuel cells operation are essential for understanding the PV characteristics curves, power output and hourly hydrogen production, such as the FC performance and the payback time. Hence, the main objective of the present study is to perform energy and exergy analysis of a hybrid system with PV panels, electrolyzer and SOFC. Based on the hourly solar irradiation and hourly demand profiles during the summer, winter and spring seasons, a numerical simulation developed in MATLAB software evaluates the technical feasibility of this system in the district of Xerém, located in the city of Duque de Caxias, state of Rio de Janeiro, Brazil. Also, an economical feasibility analysis is considered for future work, as it should be the critical point to make the installation of the hybrid system viable.

2. SYSTEM DESCRIPTION

The studied system consists in PV panels, electrolyzer and a SOFC coupled in a small-scale residence for electric supply purpose. Figure 1 illustrates the hybrid system, as well as the fuel storage, load controller, current converter and the power load.

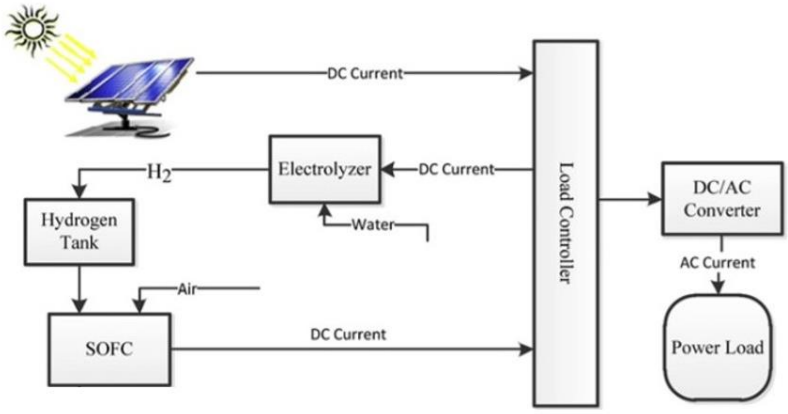

Figure 1. Schematic of the solar PV-hydrogen SOFC system for residential applications (adapted from Hosseini *et al.*, 2013).

The PV panels provides a direct current that goes to a load controller that sends the required power to the residence and the eventual power surplus to the electrolyzer for hydrogen production, accordingly to the hourly electric demand. It

is selected a low temperature PEM water electrolyzer due to its shorter response time to load variations, compared to SOFCs. Therefore, the PEM electrolyzer responds faster to load and solar availability variations. When the demand surpasses than the PV power, the SOFC consumes the hydrogen from the storage tank and oxygen from the air to produce electricity and high temperature gases – that can be used in a heat recovery steam generation unit. The PV and SOFC power output are converted in a DC/AC inverter to meet the power requirements of the house.

The recorded data for solar irradiance in Xerém in summer, winter and spring was collected from a meteorological station, as shown in Fig. 2. Additionally, the feasibility of this hybrid system was tested for a high consumption residence consumer with an average monthly consumption of 1344 kWh, based on Gabriel (2020), as presented in Fig. 3.

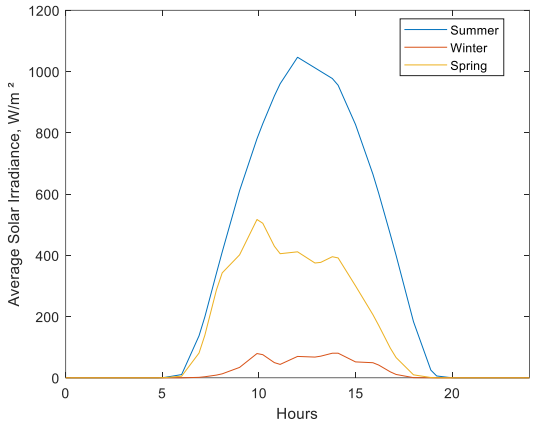

Figure 2. Hourly solar irradiance as a function of the hour of the day.

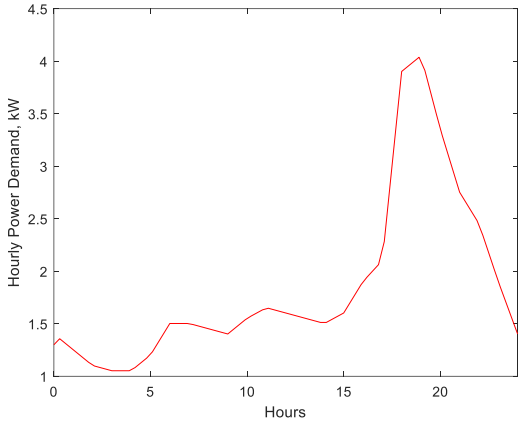

Figure 3. Hourly electric power demand as a function of the hour of the day.

3. ANALYSIS

In order to model system, the following assumptions are made:

- The hybrid system always operates at steady-state conditions.
- Possible sources of data noise, e.g. sudden changes in solar irradiance and electric power demand, are not considered in the analyses (i.e. average values are used).
- The PV panels are well maintained, so their performance is not affected by dust accumulation.
- Heat losses from the system boundary are not considered.
- Temperature at the SOFC input channels is 100K lower than the temperature at the exit channels.
- Temperature of the SOFC solid structure is midway between the inlet and exit temperatures.
- Contact resistances ($R_{contact}$) in the fuel cell are ignored.
- Radiation transfer between solid structure and gas channels is not modelled.

3.1 Photovoltaic system

The PV cells performance reveals non-linear current-voltage (I–V) characteristic curves. The reference literature presents comprehensive models of PV systems where the I–V characteristic curve was expressed as (HOSSEINI *et al.*, 2013)

$$I_{PV} = I_L + I_0 \left[\exp\left(\frac{q(V_{PV}+IR_S)}{\gamma k T_{cell}}\right) - 1\right], \quad (1)$$

where I_{PV} is the current (A), I_L is the light current (A), I_0 is the reverse saturation current (A), q is the electron charge (C), V_{PV} is the voltage (V), R_S is the series cell resistance (Ω) accordingly to MASOUM *et al*. (2002), γ is the shape factor, k is the Boltzmann constant (J/K) and T_{cell} is the cell temperature (K).

The light current (I_L) of Eq. (1) depends on solar irradiance and temperature, as seen in Eq. (2):

$$I_L = \left(\frac{G}{G_{ref}}\right) \cdot \left(I_{L,ref} + k_t\left(T_{cell} - T_{ref}\right)\right), \quad (2)$$

where G is the solar insolation (W/m²), G_{ref} is the solar insolation at the design condition, $I_{L,ref}$ is calculated based on the manufacturer data for short-circuit and maximum point currents, k_t is the manufacturer supplied temperature coefficient of short-circuit current (A/ºC) and T_{ref} is the reference temperature (K).

The Eq. (3) presents the reverse saturation current (I_0) as a function of cell temperature and material band gap energy.

$$I_0 = I_{L,ref} \exp\left(-\frac{qV_{oc}}{\gamma k T_{ref}}\right)\left(\frac{T_{cell}}{T_{ref}}\right)^3 \exp\left[\left(\frac{q\varepsilon}{k\alpha}\right)\left(\frac{1}{T_{ref}} - \frac{1}{T_{cell}}\right)\right], \quad (3)$$

where V_{oc} is the open-circuit voltage (V), ε is the material band gap energy (1.12 eV for silicon cells) and α is the completion or ideality factor, accordingly to ONAR *et al*. (2008).

The shape factor (γ) in Eq. (1) is a measure of cell imperfection and is related to the completion factor (α) as

$$\gamma = \alpha \cdot NCS \cdot NS, \quad (4)$$

where NCS corresponds to number of cells in module and NCS to number of modules in series.

As seen in Eq. (1), external factors can impact in the PV system performance, such as the cell temperature being affected by reference temperature in Eq. (2). Thus, the Eq. (5) presents the influence of some external factors on the cell temperature, as ambient temperature, wind speed and total solar irradiance.

$$T_{cell} = 0.943T_0 + 0.028G - 1.528V_{wind} + 4.3, \quad (5)$$

where T_0 is the ambient temperature (K) and V_{wind} is the wind speed (m/s).

The PV module specifications are the same as studied by Hosseini *et al.* (2013), shown in Tab. 1.

Table 1. PV module specifications, adapted from Hosseini *et al.* (2013)

Short-circuit current, I_{SC} (A)	5.75
Open-circuit voltage, V_{OC} (V)	47.7
Array area, A_{PV} (m²)	1.244
Number of cells in module, NCS	72
Number of modules in series, NS	7
Number of modules in parallel, NP	7
Reference conditions	
Total irradiance, G_{ref} (W/m²)	1000
Wind speed, V_{wind} (m/s)	5
Ambient temperature, T_0 (ºC)	25

The PV cell power output (P_{PV}) is the product between current (I) and voltage (V), as seen in Eq. (6). Furthermore, the solar energy and exergy flow rates are calculated in Eqs. (7) and (8), respectively, in order to determinate efficiencies, since the PV system efficiency is the conversion rate of solar energy to electric energy.

$$P_{PV} = I_{PV} \cdot V_{PV}, \quad (6)$$

$$\dot{En}_{solar} = G \cdot A_{PV} \cdot NS \cdot NP, \quad (7)$$

$$\dot{Ex}_{solar} = G \cdot A_{PV} \cdot NS \cdot NP \cdot \left(1 - \frac{4}{3}\frac{T_0}{T_{sun}} + \frac{1}{3}\left(\frac{T_0}{T_{sun}}\right)^4\right), \quad (8)$$

where P_{PV} corresponds to the PV power output (J), $\dot{En}_{solar}$ to the solar energy flow rate (W), $\dot{Ex}_{solar}$ to the solar exergy flow rate (W), A_{PV} to the array area (m²), NP to the number of modules in parallel and T_{sun} to the sun temperature (K).

Based on the non-linear characteristic of Eq. (1), a maximum power output can be obtained, which will be used in the numerical simulation of this study. Hence, the corresponding current and voltage values are called I_{mp} and V_{mp}, and the subsequent power output is P_{mp}. Moreover, the PV system is designed to operate at the maximum power point throughout its operation.

Therefore, the Eqs. (9) and (10) present the energy and exergy efficiencies of the photovoltaic system.

$$\eta_{PV} = \frac{P_{PV}}{\dot{En}_{solar}} = \frac{P_{mp}}{\dot{En}_{solar}}, \quad (9)$$

$$\psi_{PV} = \frac{P_{PV}}{\dot{Ex}_{solar}} = \frac{P_{mp}}{\dot{Ex}_{solar}}. \quad (10)$$

3.2 DC/AC inverter

The energy efficiency of the DC/AC inverter is considered constant and equal to 96% (HOSSEINI *et al*., 2013).

3.3 Water electrolyzer

The surplus electricity from the photovoltaic system, P_{el}, supplies both electrolysis and compression of the gas produced. The produced hydrogen flow rate is calculated from the PEM water electrolyzer energy efficiency, equal to 65% (HOSSEINI *et al*., 2013), while the gas compression consumes 0.7 kWh/kg of produced hydrogen (YANG and OGDEN, 2007).

$$\eta_{el} = \frac{\dot{m}_{H_2} \cdot LHV_{H_2}}{P_{el}}, \quad (11)$$

where $\dot{m}_{H_2}$ is the hydrogen flow rate (kg/s), LHV_{H_2} is the hydrogen lower heating value (33 kWh/kg, according to the Office of Energy Efficiency & Renewable Energy) and the P_{el} is the power input to the electrolyzer (J).

3.4 Solid oxide fuel cell

Figure 4 presents a schematic representation of the simulated fuel cell, in which part of the exiting gas at the cathode recirculates to reduce the consumption of fresh hydrogen (Colpan *et al*., 2007).

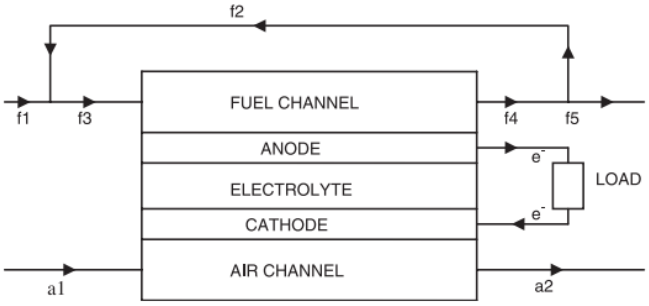

Figure 4. Schematic representation of the SOFC (Colpan *et al.*, 2007).

The hydrogen enters the fuel channel with recirculated gas (hydrogen and water, since the chemical reactions produce water as product) and undergoes the FC anode, where reacts electrochemically with the oxygen from the cathode. The hydrogen consumption rate depends on the fuel cell current density, fuel utilization rate and recirculation rate.

For the insulated fuel cell, the energy balance around the control volume enclosing the fuel cell is written as

$$\sum \dot{N}_{f1}^{i} \cdot \bar{h}^{i}\left(T_{f1}\right) = \sum \dot{N}_{f3}^{i} \cdot \bar{h}^{i}\left(T_{f3}\right) - \sum \dot{N}_{f2}^{i} \cdot \bar{h}^{i}\left(T_{f2}\right), with\ \bar{h}^{i}(T) = \bar{h}^{\circ}_{f,i} + \int_{298}^{T}(a_i + b_i T + c_i T^2 + d_i T^3)dT, \quad (12)$$

where $\dot{N}_j^i$ is the molar flow rate of the specie i in the current j (mol/s), $\bar{h}^i$ is the specific molar enthalpy of the specie i (J/mol), T_j is the temperature in the current j (K). Jarungthammachote et al. (2007) define $\bar{h}^{\circ}_{f,i}$ as the enthalpy of formation of the gas i (kJ/kmol), and a_i, b_i, c_i and d_i stand to the coefficients of specific heat of the gas i.

Here, the enthalpy flow rate of state 'f_1' is calculated using an energy balance around the control volume enclosing the junction point by Eq. (13). The temperature of this state is then found by iteration:

$$\sum \dot{N}_{f1}^{i} \cdot \bar{h}^{i}\left(T_{f1}\right) + \sum \dot{N}_{a1}^{j} \cdot \bar{h}^{j}(T_{a1}) = \dot{W}_{SOFC} + \sum \dot{N}_{f5}^{i} \cdot \bar{h}^{i}\left(T_{f5}\right) + \sum \dot{N}_{a2}^{j} \cdot \bar{h}^{j}(T_{a2}), \quad (13)$$

where $\dot{W}_{SOFC}$ is the SOFC output power (W).

The molar flow rates of gas species at the air channel inlet and exit, as well as the extent of electrochemical reaction, c, are defined as

$$\dot{N}_{a1}^{O_2} = \frac{c}{2 \cdot U_{ox}}, \dot{N}_{a1}^{N_2} = \frac{79}{42} \cdot \frac{c}{U_{ox}}, \dot{N}_{a2}^{O_2} = \frac{c}{2}\left(\frac{1}{U_{ox}} - 1\right), \dot{N}_{a2}^{N_2} = \frac{79}{42} \cdot \frac{c}{U_{ox}}, with\ c = \frac{\dot{N}_{f1}^{H_2} \cdot U_F}{1 - r + U_F \cdot r}, \quad (14)$$

where c is the extent of electrochemical reaction (mol/s), U_{ox} is the air (oxidant) utilization ratio, U_F is the fuel utilization ratio and r is the recirculation ratio.

Hence, the molar concentrations of the air mix in the air exit channel are calculated as

$$x_{a2}^{O_2} = \frac{\dot{N}_{a2}^{O_2}}{\dot{N}_{a2}} = \frac{1 - U_{ox}}{{}^{100}/_{21} - U_{ox}}, x_{a2}^{N_2} = 1 - x_{a2}^{O_2}, \quad (15)$$

where x_j^i is the molar concentration of the specie i in the current j.

The SOFC current is calculated as Eq. (16) defines, in which the current density relates to the SOFC area.

$$I_{SOFC} = i \cdot A_{SOFC} = 2 \cdot F \cdot c = 2 \cdot F \cdot \frac{\dot{N}_{f1}^{H_2} \cdot U_F}{1 - r + U_F \cdot r}, \quad (16)$$

where I_{SOFC} is the SOFC current (A), i is the current density (A/cm²), A_{SOFC} is the SOFC activate surface area (cm²) and F is the Faraday constant (C).

Here, three types of polarizations – ohmic, activation and concentration – and the Nernst voltage result in the SOFC voltage, as seen through Eqs. (17) – (23).

$$V_{SOFC} = V_N - V_{ohm} - V_{act} - V_{conc}, \quad (17)$$

where V_{SOFC} is the SOFC voltage (V), V_N is the Nernst voltage (V), V_{ohm}, V_{act} and V_{conc} are, respectively, the ohmic, activation and concentration polarizations (V).

The Nernst voltage is calculated as

$$V_N = \frac{-\Delta\bar{g}^\circ_T}{2F} - \frac{RT_{exit}}{2F} \cdot ln\left(\frac{x_{f4}^{H_2O}}{x_{f3}^{H_2} \cdot \sqrt{x_{a1}^{O_2} \cdot P/P^\circ}}\right), \quad (18)$$

$$with\ \Delta\bar{g}^\circ_T = \sum_i v_i\,(\bar{h}^\circ_f - a'T_{SOFC}\,ln(T_{SOFC}) - b'T_{SOFC}^2 - \left(\frac{c'}{2}\right)T_{SOFC}^3 - \left(\frac{d'}{3}\right)T_{SOFC}^4 + \left(\frac{e'}{2\cdot T_{SOFC}}\right) + f' + g'T_{SOFC}), \quad (19)$$

where $\Delta\bar{g}^\circ_T$ is the change in specific molar Gibbs free energy (J/mol), R is the universal gas constant (J/mol·K), P is the pressure (bar) and P° is the standard state pressure (bar). Also, v_i is the reactions stoichiometric number, and a' to g' are the coefficients of the empirical equation for $\Delta\bar{g}^\circ_T$ (Jarungthammachote et al., 2007).

Furthermore, the ohmic polarization is caused by the resistance to the flow of oxide ions through the electrolyte and resistance to the flow of electrons. The activation polarization is the voltage drop due to the sluggishness of reactions occurring at the electrode–electrolyte interfaces. If it is assumed that charge transfer coefficient for anode and cathode is 0.5 and substitute this value in the Butler–Volmer equation, this equation takes the form as shown in Eq. (21). The concentration polarization is caused by the resistance to mass transport through the electrodes and interfaces (Colpan *et al.*, 2007).

$$V_{ohm} = (R_{contact} + \sum_k \rho_k \cdot L_k) \cdot i, \quad (20)$$

$$V_{act} = V_{act,a} + V_{act,c} = \frac{RT_{SOFC}}{F} \cdot sinh^{-1}\left(\frac{i}{2i_a}\right) + \frac{RT_{SOFC}}{F} \cdot sinh^{-1}\left(\frac{i}{2i_c}\right), \quad (21)$$

$$V_{conc} = V_{conc}^a + V_{conc}^c = \left[-\frac{RT_{exit}}{2F} ln\left(1 - \frac{i}{i_{lim,a}}\right) + \frac{RT_{exit}}{2F} ln\left(1 + \frac{P_{f4}^{H_2} \cdot i}{P_{f4}^{H_2O} \cdot i_{lim,a}}\right)\right] + \left[-\frac{RT_{exit}}{4F} ln\left(1 - \frac{i}{i_{lim,c}}\right)\right], \quad (22)$$

$$with\ i_{lim,a} = \frac{2 \cdot F \cdot P_{f3}^{H_2} \cdot D_{dif,a}}{R \cdot T_{exit} \cdot L_a}\ and\ i_{lim,c} = \frac{4 \cdot F \cdot P_{a2}^{O_2} \cdot D_{dif,c}}{\left(\left(P - P_{a2}^{O_2}\right)/P\right) \cdot R \cdot T_{exit} \cdot L_c}, \quad (23)$$

where $R_{contact}$ is the contact resistances (Ω), ρ_k is the electrical resistivity of cell component k (Ω .cm), L_k is the electrical resistivity of cell component k (μm), i_a and i_c are, respectively, the exchange current density of anode and cathode, (A/cm²), $i_{lim,a}$ and $i_{lim,c}$ are the anode and cathode limiting current density, respectively (A/cm²). Also, P_j^i is the pressure of the specie i in the current j (bar), and $D_{dif,a}$ and $D_{dif,c}$ are the effective gaseous diffusivity through the anode and the cathode, respectively (cm²/s).

The SOFC input parameters, shown in Tab. 2, are those adopted by Hosseini *et al.* (2013).

Table 2. Input parameters to the SOFC model, adapted from Hosseini *et al.* (2013) and Colpan *et al.* (2007)

Inlet air temperature (°C)	25
Inlet channel temperature (ºC)	750
Exit channel temperature (ºC)	850
Stack temperature (°C)	800
Activation area (cm²)	834
Cell current density (A/cm²)	0.3
Fuel Utilization	0.85
Number of cells	15

The internal consumption of the SOFC balance of plant is considered to be 4% of the generated power. Therefore, knowing that the SOFC power, $\dot{W}_{SOFC}$, is the product between the current and voltage, Eq. (24) presents the net electric power output of the fuel cell.

$$\dot{W}_{net-SOFC} = \dot{W}_{SOFC} - \dot{W}_{consumption} = 0.96 \cdot \dot{W}_{SOFC}\,, \quad (24)$$

where $\dot{W}_{consumption}$ accounts for the internal consumption of the fuel cell system, e.g. air blower, control system, etc.

Finally, the energy and exergy efficiencies for the fuel cell are

$$\eta_{SOFC} = \frac{\dot{W}_{net-SOFC}}{\dot{m}_{H_2,SOFC} \cdot LHV_{H_2}}\,, \quad (25)$$

$$\psi_{SOFC} = \frac{\dot{W}_{net-SOFC}}{\dot{m}_{H_2,SOFC} \cdot ex_{H_2}}\,. \quad (26)$$

where $\dot{m}_{H_2,SOFC}$ is the hydrogen mass flow rate into the SOFC (g/s) and ex_{H_2} is the hydrogen specific exergy (kJ/kg).

Finally, if the PV system is in operation and the power surplus is directed to the electrolyzer for hydrogen production, the total efficiencies are calculated as:

$$\eta_{total} = \frac{\int\left(P_{demand} + \dot{m}_{H_2} \cdot LHV_{H_2}\right) dt}{\int(\dot{E}n_{solar})dt + m_{H_2,i} \cdot LHV_{H_2}}\,, \quad (27)$$

$$\psi_{total} = \frac{\int\left(P_{demand} + \dot{m}_{H_2} \cdot ex_{H_2}\right) dt}{\int(\dot{E}x_{solar})dt + m_{H_2,i} \cdot ex_{H_2}}\,. \quad (28)$$

where $m_{H_2,i}$ is the initial hydrogen storage (g).

4. RESULTS AND DISCUSSION

The PV power output has a maximum point – according to the I–V characteristic curve –, after which the power drops significantly. The simulated PV systems are designed to operate at the maximum power point with the solar radiation variation (Hosseini *et al.*, 2013). Therefore, Figure 5 presents the PV power output, responsible for supplying the hourly demand, and, if it exceeds it, it is converted into hydrogen in the water electrolysis.

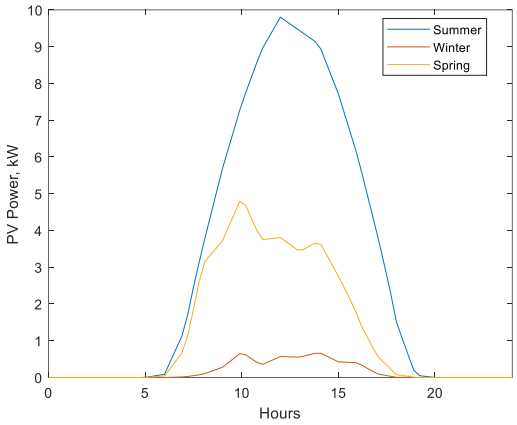

Figure 5. Variation of the PV power output as a function of the hour of the day.

As can be seen in the graphic, the PV power follows the same trend as the solar irradiance in Fig. 2. Also noteworthy the very high PV electric power produced during summer, reaching 9.8 kW, while in winter the values do not exceed 1 kW. It will be observed how the discrepancy between the summer, winter and spring data will affect the final results.

Now, it is evaluated if the PV power output is able to supply the electric demand. Thus, the difference between these two data is calculated, as seen in Fig. 6. If the difference is positive, hydrogen is produced by electrolysis. However, if it is not, there is an hydrogen consumption in the SOFC for the electric supply.

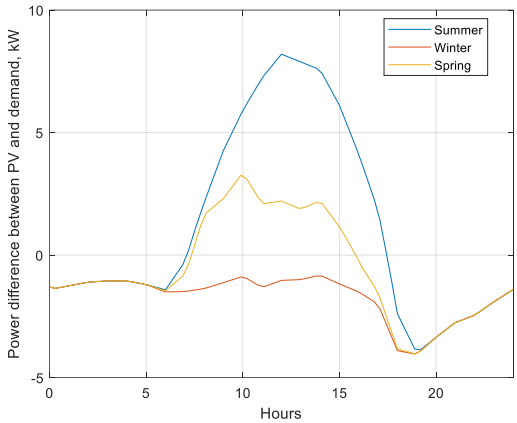

Figure 6. Evolution of the energy surplus as a function of the hour of the day.

This graphic requires a careful analysis. The positive values of the summer and spring indicate a PV output higher than the demand during the day, when hydrogen will be produced and stored for the later consumption in the SOFC. However, during winter, there is only negative values, concluding that hydrogen will not be produced in the electrolysis since there is no excess power, nor the SOFC operation, which depends on the fuel.

Figure 7 presents the hydrogen production during the studied seasons.

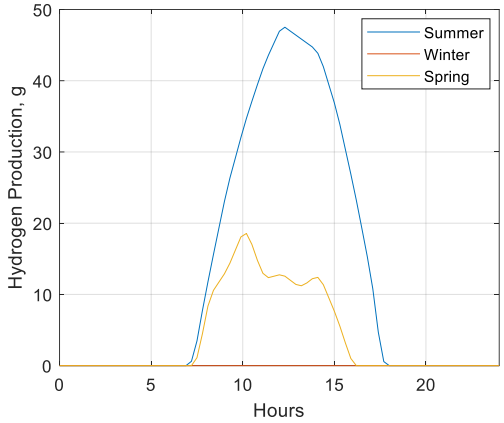

Figure 7. Hydrogen production in the electrolyzer as a function of the hour of the day.

The hydrogen production during summer and spring corresponds to the positive values of the difference between the PV power and the demand during the same seasons, as expected. It is relevant to observe the absence of hydrogen production during winter, as discussed previously. It is also important to calculate the hydrogen accumulation over the day, as it is produced during the electrolyzer operation. Figure 8 presents these data, which will be used to evaluate if the hydrogen amount is enough to supply the SOFC demand.

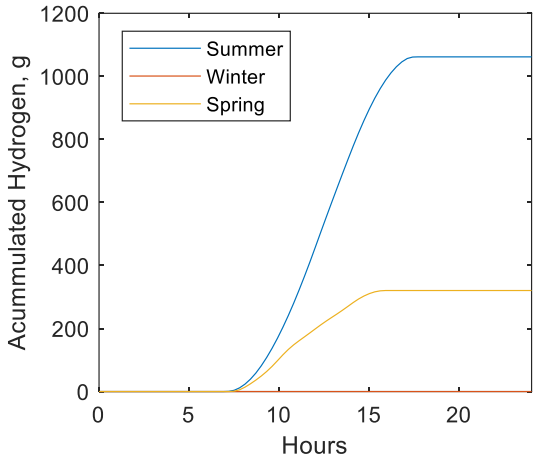

Figure 8. Amount of hydrogen accumulated broken down by hour of the day.

Thus, disregarding the SOFC hydrogen consumption at this analysis, during the summer there is storage of 1.062 kg of hydrogen, much higher than the 0.7 kg studied by HOSSEINI *et al.* (2013) in the same season. During spring, there's the accumulation of more than 0.3 kg, while in winter it remains nil.

Consequently, knowing the amount of stored hydrogen available, it is studied the SOFC operation in order to assess whether the gas produced and stored is sufficient. Figure 9 addresses the SOFC fuel consumption throughout the day, for the studied seasons.

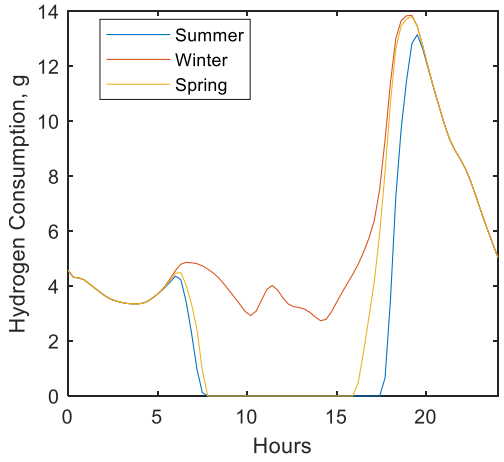

Figure 9. SOFC hydrogen consumption broken down by hour of the day.

It is relevant to observe the qualitative similarity of the hydrogen consumption with the electric demand seen in Fig. 3. During the winter, the hydrogen consumption is always positive, as seen in the red curve. Since PV power is not capable to meet the electric demand, another power supply is required, which, in this case, would be the hydrogen. As observed in the negative values in Fig. 5, there is always this positive demand for hydrogen during the winter, when the SOFC needs to provide the necessary power. However, as presented, there is no hydrogen production at this period of the year, so it would be necessary to use grid electricity to supply the demand.

In order to evaluate the final hydrogen availability, it is calculated its balance after the SOFC consumption, as seen in Fig. 10. So that there are no negative balance values, it is assumed that there is an initial hydrogen storage of 451.9 g.

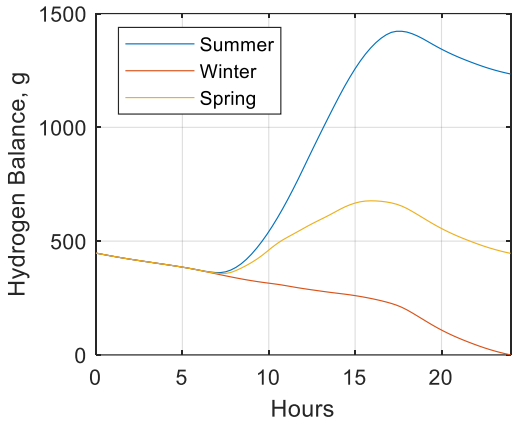

Figure 10. Total hydrogen balance as a function of the hour of the day.

The final balance of hydrogen during summer reaches 1.234 kg – with an initial storage of 451.9 g –, highlighting the very high feasibility of the proposed configuration. During spring, the final balance is very close of the initial amount, indicating a slow consumption of the stored hydrogen. In winter, there would be a total consumption of the fuel initially stored, however, it is reinforced that in under real conditions, the electricity demand should be provided from the grid.

Finally, the energy and exergy analysis of both the PV system and the fuel cell is performed, as presented in Figs. 11 and 12, respectively. For these analysis, the recirculation and fuel utilization ratios values were fixed, at 0.3 and 0.85, respectively. Posteriorly, it is evaluated how its variation affect the efficiencies.

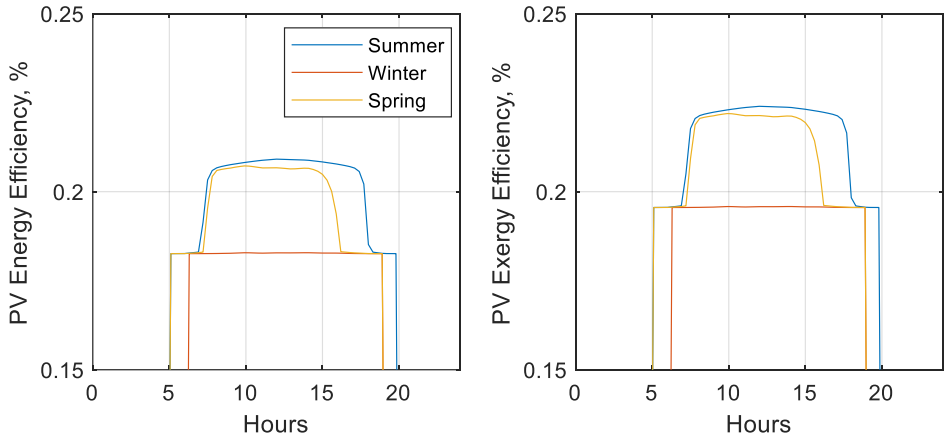

Figure 11. PV energy and exergy efficiencies as a function of the hour of the day.

The PV energy efficiency ranged from 18 to 21% while the exergy efficiency is slightly higher (19 to 23%). The maximum efficiency is found during summer when the irradiation is at its maximum, while during winter, it is lower due to the low solar irradiation and almost constant. Such behavior is expected from the I–V characteristic curve as a function of the incident energy.

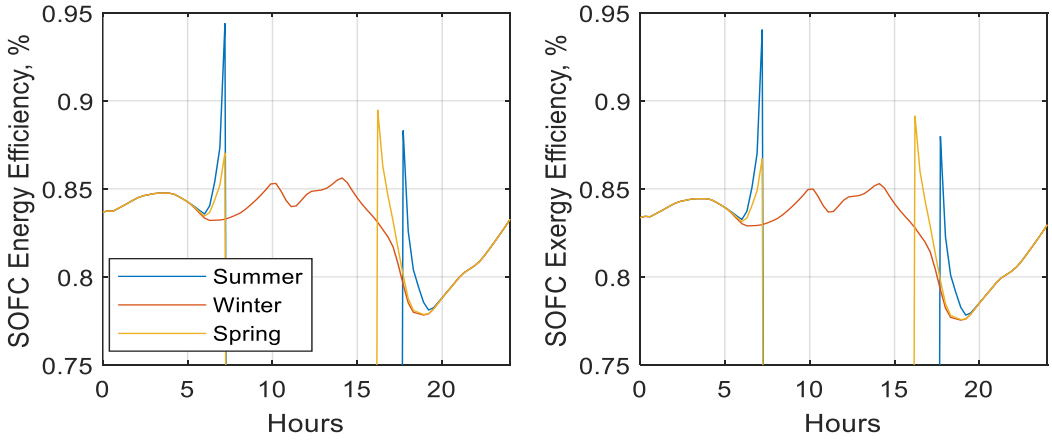

Figure 12. SOFC energy and exergy efficiencies as a function of the hour of the day.

In summer and spring, the efficiencies drop (in fact, is null) during the day since the PV fully provide the energy load and the fuel cell is shut down. During winter, the PV does not produce enough power to supply the demand, than it is require the SOFC operation during this period of the day. That explains that the SOFC was not shut down during winter.

Furthermore, it is important to understand how the recirculation ratio and the fuel utilization ratio impact in the efficiencies. Thus, with these parameters fixed at 0.3 and 0.85 respectively, the maximum energy and exergy efficiencies of the SOFC system are 94.38% and 94.03%, respectively. In the worst case, with a 10% recirculation ratio and 65% fuel utilization ratio return 72.76% and 72.49% of maximum energy and exergy efficiencies, respectively. These analysis show that the higher those parameters used in the SOFC, the higher the efficiencies reach, both on maximum points and at the others periods of the day.

5. CONCLUSIONS

This paper studied the hourly power generation of a hybrid system with PV panels, electrolyzer and SOFC, in order to evaluate its energy and exergy efficiencies and its technical feasibility. For the available solar irradiance in Xerém, located in Duque de Caxias, 1.062, 0.320 and 0.0 kg/day hydrogen is produced with the surplus electricity of the PV system, during summer, spring and winter, respectively. The SOFC meets the power demand of the house during solar unavailability. The maximum energy and exergy efficiencies of the photovoltaic system are 20.9% and 22.4%, respectively. Moreover, the maximum energy and exergy efficiencies of the SOFC system are 94.38% and 94.03%, respectively. The total efficiency of the PV-hydrogen SOFC system is related to the pattern of the power demand and solar availability. The maximum total energy efficiency is reported as 35.75%, while the maximum total exergy efficiency is 38.38%, both during summer. These results are obtained for the hours that the fuel cell is in operation.

Such results are optimistic since no heat loss are considered in the fuel cell. In future works, a more detailed model of the SOFC fuel cell, including heat transfer, kinetics and transient regime should be studied to provide more realistic results. The current model should also be applied as a base for a study of the economic viability of the project in a long term perspective (25 years).

6. ACKNOWLEDGMENTS

The authors are indebted to CNPq/MCT and CAPES for the financial support to the Department of Mechanical Engineering (DEM) at the Pontifical Catholic University of Rio de Janeiro (PUC-Rio).

7. REFERENCES

Colpan, C.O., Dincer, I., Hamdullahput, F., 2007. “Thermodynamic modeling of direct internal reforming solid oxide fuel cells operating with syngas”. *International Journal of Hydrogen Energy*, Vol. 32, pp 787-795.

Dutta, S., 2014. “A review on production, storage of hydrogen and its utilization as an energy resource”. *Journal of Industrial and Engineering Chemistry*, Vol. 20, pp 1148-1156.

Gabriel. R.O., 2020. *Energetic, economic and environmental analysis of a micro-CHP with fuel cell using natural gas and photovoltaic panels for residential and industrial appliance* (in Portuguese). Master Dissertation. Department of Mechanical Enginnering. Pontifícia Universidade Católica do Rio de Janeiro, Rio de Janeiro, RJ – Brazil.

Hosseini, M., Dincer, I., Rosen, M. A., 2013. “Hybrid solar-fuel cell combined heat and power systems for residential applications: Energy and exergy analyses”. *Journal of Power Sources*, Vol. 221, pp 372–380.

Jarungthammachote, S., Dutta, A., 2007. “Thermodynamic equilibrium model and second law analysis of a downdraft waste gasifier”. *Energy*, Vol. 32, pp 1660–1669.

Office of Energy Efficiency & Renewable Energy. *Hydrogen Storage*, https://www.energy.gov/eere/fuelcells/hydrogen-storage. Acessed 18 June 2021.

Onar, O.C., Uzunoglu, M., Alam, M.S., 2008. "Modeling, control and simulation of an autonomous wind turbine/photovoltaic/fuel cell/ultra-capacitor hybrid power system". *Journal of Power Sources*, Vol. 185, pp 1273–1283.

Sauthier, L.F., Diefenthäler, A.T., Sausen, P.S., Sausen, A.T., de Campos, M., Walker, G., 2019. *Mathematical modeling of photovoltaic modules used in simulations environments of distributed generation* (in Portuguese). Universidade Regional do Noroeste do Estado do Rio Grande do Sul, Ijuí, Rio Grande do Sul

Sharaf, O.Z., Orhan, M.F., 2014. "An overview of fuel cell technology: Fundamentals and applications". *Renewable and Sustainable Energy Reviews*, Vol. 32, pp 810-853.

Tao, J., Yu, S., 2015. "Review on feasible recycling pathways and technologies of solar photovoltaic modules". *Solar Energy Materials & Solar Cells*, Vol. 141, pp 108–124.

Ursúa, A., Gandía, L.M., Sanchis, P., 2012. "Hydrogen Production from Water Electrolysis: Current Status and Future Trends". *Proceedings of the IEEE*, Vol. 100, No. 2.

Yang, C., Ogden, J., 2007. "Determining the lowest-cost hydrogen delivery mode". *International Journal of Hydrogen Energy*, Vol. 32, pp 268-286.

8. RESPONSIBILITY NOTICE

The authors are the only responsible for the printed material included in this paper.